NACA RM L50B01

NACA

RESEARCH MEMORANDUM

PRELIMINARY INVESTIGATION OF CONSTANT-GEOMETRY, VARIABLE MACH NUMBER, SUPERSONIC TUNNEL WITH POROUS WALLS

By William J. Nelson and Paul L. Klevatt

Langley Aeronautical Laboratory
Langley Air Force Base, Va.

NATIONAL ADVISORY COMMITTEE
FOR AERONAUTICS

WASHINGTON

May 3, 1950

NACA RM L50B01

NATIONAL ADVISORY COMMITTEE FOR AERONAUTICS

RESEARCH MEMORANDUM

PRELIMINARY INVESTIGATION OF CONSTANT-GEOMETRY, VARIABLE MACH NUMBER, SUPERSONIC TUNNEL WITH POROUS WALLS

By William J. Nelson and Paul L. Klevatt

SUMMARY

A method of generating variable Mach number supersonic flow in a channel of fixed geometry by the removal of air through uniform porous walls is discussed. Calculated porosity distributions are presented for several minimum-length nozzles designed to operate at Mach numbers up to 2.0. The axial pressure gradient has been calculated for several constant-porosity walls over a range of Mach numbers. The applicability of these calculations to a two-dimensional tunnel is illustrated by comparison of calculated and experimentally determined pressure gradients in the $2\frac{1}{4}$- by $4\frac{1}{2}$-inch channel at Mach numbers in the range covered in the present tests, 0.99 to 1.17. Schlieren photographs of the flow in the experimental channel are also presented.

INTRODUCTION

The development of variable Mach number supersonic wind tunnels has received a great deal of attention during recent years. Several schemes for varying the Mach number by changing the tunnel geometry have been tried. These include moving nozzle blocks (references 1, 2, and 3) and flexible walls (references 4 and 5). Another type of variable Mach number wind tunnel being investigated by the National Advisory Committee for Aeronautics and others utilizes a series of longitudinal slots in fixed tunnel walls. In these fixed-geometry tunnels the Mach number is varied by changing the pressure in the slots relative to the

the stream stagnation pressure. Preliminary results of this work are available in references 6 to 9.

The present investigation is a continuation of the slotted-tunnel work but utilizes porous metallic walls rather than a finite number of passages as employed in the slotted tunnels. Either the slotted or the porous-wall tunnels offer the possibility of avoidance of transonic choking in addition to variation of the supersonic Mach number with fixed geometry. Research on both possibilities is in progress, but the present paper is concerned only with the problem of variable supersonic Mach number. This report contains a simplified analysis of the tunnel-wall characteristics required to generate shock-free supersonic flow in minimum distance together with calculated and experimental pressure distributions along a constant-cross-section channel with walls of known porosity. All calculations were based upon the methods which are discussed in reference 10 using tabular data from reference 11. The experimental data presented were obtained in a symmetrical channel of rectangular cross section $\left(2\frac{1}{4} \text{ by } 4\frac{1}{2} \text{ inches}\right)$. This work was done under steady-flow conditions with air supplied at elevated pressures while atmospheric pressure was maintained in the area surrounding the tunnel. The work was initiated at the Langley internal aerodynamics section in the summer of 1948 and is continuing.

SYMBOLS

a	sonic velocity
g	acceleration due to gravity
p	local static pressure
Δp	local pressure difference across porous surface
M	local Mach number
V	velocity
δ	angle of flow relative to wall
γ	ratio of specific heats
ρ	mass density
ν	cumulative sum of expansive deviations of stream from direction of flow at $M = 1.0$
x	distance along porous section

h height of channel

Subscripts

D design condition

o stagnation condition

n component normal to porous wall

ANALYSIS

The difference in Mach number between any two points in a two-dimensional supersonic tunnel bears a unique relationship to the cumulative sum of the angular deviations to which the stream has been subjected between those points. A complete discussion of the relationship between the Mach number and stream deviation can be found in reference 10, chapter 2. If the direction of flow at $M = 1.00$ is taken as a basis of reference, this relationship may be expressed as

$$\nu = \left(\frac{\gamma + 1}{\gamma - 1}\right)^{1/2} \cos^{-1}\left[\frac{\gamma + 1}{2\left(1 + \frac{\gamma - 1}{2}M^2\right)}\right]^{1/2} + \sin^{-1}\frac{1}{M} - 90^\circ$$

The generation of supersonic Mach numbers in conventional tunnels is accomplished by accelerating the air stream in a Laval type nozzle; the rate of acceleration and therefore the length of the tunnel being determined by the curvature of the walls. In a symmetrical, minimum-length, shock-free nozzle, one-half the design stream deviation ν_D corresponding to the final Mach number M_D is produced by increasing the angle between the wall and the center line of the stream at a point; the remaining deviation, a result of the initial stream curvature along the opposite wall, produces a realinement of the flow to the tunnel center line. For the purposes of this analysis only the flow in the lower half of a symmetrical nozzle will be considered, thus, for the Mach number range under discussion, all characteristics with positive slope are defined as part of the first family expansion while those characteristics with negative slope are from the second family expansion, figure 1.

Shock-free nozzles.- By initiating the first family expansion at a point and curving the wall downstream of this point to correspond to the

direction of flow through the second family expansion, the design Mach number will be reached in the minimum distance with continuous acceleration of the stream. The resulting nozzle is of the general type shown in the characteristic diagram of figure 1. Along the tunnel wall the velocity component normal to the tunnel axis increases from 0 to a maximum at a value corresponding to $\nu_D/2$ at the point of initial turning; continued acceleration of the stream beyond this point is accomplished by curvature of the streamlines in the opposite direction with resulting reduction in the normal component to zero. The magnitude of these velocity components is shown for several minimum-length nozzles in figure 2(a). The curves, drawn as a function of ν, are for completeness presented for both first and second family expansions although the region of practical interest is limited to that section of the curves drawn double weight. If the solid wall is replaced by a porous wall parallel to the plane of symmetry, the velocity component normal to the tunnel axis becomes the component normal to this wall; if the porosity of the wall is such that this flow may pass through the wall, minimum-length nozzle flow will be realized. The pressure variation as a function of ν is also shown in figure 2(a).

The rate of flow through any porous material is determined by the pressure difference across it and by its loss characteristics; thus, any flow distribution can be obtained by a suitable matching of the pressure differential across the material and its loss characteristics. The following analysis is based upon maintaining a constant-pressure chamber outside the porous wall and varying its resistance to flow to obtain the desired normal flow rate. Since the final pressure reached in the channel will be equal to that in the chamber outside the porous wall, the pressure increment across the wall at any point will be equal to the difference between the local static pressure and that corresponding to the design Mach number. This difference, for the shock-free nozzles of figure 2(a), is plotted in figure 2(b).

The velocity component normal to the wall and the pressure difference across it have been combined into a single parameter, $\frac{V_n/a_o}{\Delta p/p_o}$, and plotted as a function of ν in figure 3(a). As in the preceding figures, the first and second family expansions are differentiated by weight of line. For minimum-length nozzles, in which only the variation across the second family expansion is pertinent, the total change in the ordinate is relatively small until the higher Mach numbers are reached. To show the range of porosities that will be required for materials across which the pressure drop varies linearly with $\rho g V$ and $\rho g V^2$, corresponding curves

of $\frac{\frac{\rho}{\rho_o}\frac{V_n}{a_o}}{\Delta p/p_o}$ and $\frac{\frac{\rho}{\rho_o}\left(\frac{V_n}{a_o}\right)^2}{\Delta p/p_o}$ are also presented, figures 3(b) and 3(c). As in figure 3(a), these curves are, for completeness, drawn for the first family expansion as well as for the second. From a comparison of these curves it is apparent that, for a given Mach number, a material for which the relationship between Δp and $\rho g V$ remains essentially constant offers a much closer approximation to the ideal porosity than one in which Δp varies with $\rho g V^2$, since in the latter material the proportionality constant decreases to 0; this condition corresponds to a solid wall at the nozzle exit.

Curves of the ratio of the weight flow component normal to the porous wall to the pressure drop across it, $\rho g V_n/\Delta p$, as obtained from figure 3(b), are presented in figure 4 as a function of distance along the nozzle for minimum-length nozzles designed to operate at Mach numbers of 1.1, 1.2, 1.5, and 2.0. For these curves T_o was assumed constant at 500° R. From a consideration of the stagnation constants in the ordinates of figures 5(a) to 5(c), it can be seen that the porosity varies as the square root of the stagnation temperature. The length of nozzle required to generate a Mach number of 1.10 is approximately equal to one-half the tunnel height; increasing distances will be required to attain higher Mach numbers ($x = h$ for $M = 1.5$ and $x \rightarrow 2h$ for $M = 2.0$).

Corresponding curves based upon pressure drop as a function of $\rho g V_n^2$ have not been prepared since it is apparent from figure 3(c) that shock-free flows will require a wide range of porosity. Although it is possible to attain good flow with such characteristics, it appears probable that over a range of Mach numbers materials across which the pressure drop varies linearly with the mass flow will provide the more satisfactory solution.

Pressure distribution with constant porosity.- In the preceding section it was observed that the attainment of shock-free supersonic flow in a porous-walled channel requires a prescribed rate of air flow across the channel boundary. It was also shown that, for a minimum-length nozzle, the required local rate of air removal varied approximately with the first power of the difference between the local pressure and the pressure corresponding to the final Mach number. To determine the significance of departures from the calculated ideal porosity, the pressure gradient along the center line of a two-dimensional channel with walls of constant porosity $\rho g V_n/\Delta p$ has been calculated. The significance of departures from the calculated ideal porosity is shown in figures 5(a) to 5(c) where the pressure gradient along the center

line of a two-dimensional channel has been determined for walls across which the weight flow to pressure difference at $T_o = 500^\circ$ was 0.0055, 0.011, and 0.018. The pressures along a channel with walls of known porosity were determined by iteration. The normal component of the weight flow rate, $\rho g V_n$, was determined for assumed values of ν by placing $\rho g V_n = \rho g Ma \sin \delta$ and again from the known porosity by multiplying $\rho g V_n / \Delta p$ by the pressure difference corresponding to the assumed values of ν. At equilibrium, the value of $\rho g V_n$ is independent of the method of calculation; the corresponding flow angle relative to the wall was then determined from the intersection of the two curves of $\rho g V_n$ against ν. By repeating this process, the pressure distribution throughout the length of the channel was determined.

The curves presented in figure 5 show that for $\frac{\rho g V_n}{\Delta p} = 0.0055$ the distance required to reach a Mach number of 1.10 is approximately one-half the tunnel height greater than that required for the minimum-length nozzle of figure 4; for all higher Mach numbers the added distance required to reach equilibrium flow is much greater. Increasing the porosity to 0.011 (fig. 5(b)) appreciably reduces the distance required to reach equilibrium for all Mach numbers; M = 1.10 is reached in approximately the same distance required by the minimum-length shock-free nozzle; greater than minimum length is required, however, for all greater Mach numbers and since the length of the tunnel would be determined by the maximum Mach number to be reached, this porosity also is too small. At a value of $\frac{\rho g V_n}{\Delta p} = 0.018$, figure 5(c), the initial expansion is slightly excessive for Mach numbers below 1.20 but the extent of the over-expansion is small. For higher Mach numbers the distance required to reach equilibrium is somewhat in excess of the minimum although Mach numbers up to 1.5 are reached in $\frac{x}{h} < 2.0$. At higher values of $\frac{\rho g V_n}{\Delta p}$ the initial expansion at low Mach numbers is greater than that required for minimum length and subsequent compression is stronger; higher values of M can be attained, however, in very short nozzles.

APPARATUS

The general arrangement of the experimental apparatus showing a view of the test channel, the porous upper and lower walls, and the pressure tube used in making the static-pressure surveys is presented as figure 6. The contraction ratio of the entrance bell ahead of the test section was approximately 70:1. The $2\frac{1}{4}$- by $4\frac{1}{2}$-inch rectangular cross section of the

channel was constant throughout the porous region. Detailed pictures of the porous walls are presented as figure 7. These surfaces were selected commercial grade sintered bronze sheets consisting of thermally bonded bronze particles approximately 0.005 inch in diameter rolled to a thickness of 0.08 inch. The pieces used in this investigation had the smoothest surface finish of any samples readily available. The surface corresponded roughly to the surface of 120 wet-or-dry paper. Structural stiffness was provided by three longitudinal bars tapered to $\frac{1}{16}$-inch width at the point of contact with the sintered bronze; lateral support was provided at the ends only.

The $\frac{1}{8}$-inch-diameter pitot-static tube used in making the static-pressure surveys had four static orifices 0.031 inch in diameter; the total-pressure opening was 0.050 inch in diameter. Stagnation pressure and temperature were recorded at a point upstream of the entrance bell. A schlieren optical system, with 6-inch-diameter mirrors and a spark light source which produced intermittent flashes of approximately 10 microseconds, was used in photographing the flow.

EXPERIMENTAL RESULTS AND DISCUSSION

The foregoing analysis has shown the desirability of a porous material that approximates a linear variation of $\rho g V_n$ with Δp for use in generating uniform supersonic flows. Such materials, however, were not available for use in this investigation. An experimental check of this method of calculation was therefore attempted using the material at hand and calculating the pressure distribution from an experimentally determined calibration. The air flow through the sintered bronze is shown as a function of the pressure difference across the material in figure 8. The apparatus used in the calibration is shown schematically in the upper part of this figure. In applying this calibration it has been assumed that the loss characteristics are a function of the velocity component normal to the surface and are completely independent of any component parallel to the surface. The calculated pressure gradients are compared in figure 9 with the experimental pressure distributions at supersonic Mach numbers up to 1.17; this limit was established by the pressure ratios available with existing equipment and does not represent a tunnel limitation. Corresponding schlieren photographs of the flow are presented in figure 10.

In general, the experimental data are consistent with the calculated curves. Differences in absolute values of the pressure ratio as determined from calculation and experiment are, at the forward end of the nozzle, attributed to failure of the calculations to allow for

nonuniformity of flow at this point. The abrupt turn assumed in the calculations can be realized only in the absence of boundary layer at the entrance section since the presence of a layer of subsonic air at the point of turning will appreciably reduce the rate at which the flow direction may be changed. Evidence of nonuniform flow at the tunnel inlet can be found in the schlieren photographs at the left side of figure 10, where multiple shocks ahead of the porous floor $\frac{x}{h} \cong -0.4$ reach into the flow but do not completely span the channel. Experimentally determined velocity profiles at the inlet indicated that the displacement thickness of the boundary layer was approximately 0.02 inch for these tests. From one-dimensional considerations it can be shown that removal of this boundary layer alone will produce a Mach number of approximately 1.10 in the tunnel; the experimental curves would not, therefore, be expected to follow closely the calculated curves at the Mach numbers below 1.10. The reduction of the differences at the forward end of the channel between the experimental and calculated curves at $M > 1.1$ is attributed both to the reduction in boundary-layer thickness and the increase in magnitude of the initial turn. The measured pressure ratios indicate that the flow at the center line of the main stream was supersonic ahead of the porous surface for the tests at $M = 1.08$ and 1.17; this is ascribed to a thinning of the boundary layer ahead of the porous material.

Maximum deviations in Mach number of ± 0.01 are indicated by the experimental pressure distributions. Surface roughness is especially critical in this type of tunnel since supersonic velocities occur very close to the surface as a result of removal of substantial part of the air adjacent to the walls. The presence of the many Mach waves in the schlieren photographs is a result of the roughness of the sintered bronze floor. Parallelism of these waves gives some indication of the uniform velocity existing throughout the test regions. Normal shocks in the downstream section of the tunnel were caused by flow restriction at the end of the porous region where the walls were again solid.

CONCLUSIONS

The following conclusions are based upon the results of this preliminary investigation of the porosity requirements for a variable Mach number supersonic tunnel of fixed geometry:

From analysis:

(1) Shock-free supersonic flows can be obtained in a tube of constant cross section by removal of air through porous walls to a

constant-pressure chamber by proper distribution of porosity along the tunnel.

(2) The porosity requirements for shock-free nozzles vary with distance along the channel, Mach number, and with stagnation temperature.

(3) Flows possessing only small compressions can be obtained in a constant-cross-section channel by removal of air across walls of constant porosity to a chamber of constant pressure.

From experiment:

(1) The measured pressure distributions are consistent with the calculated results.

(2) The rate of expansion at the tunnel inlet is appreciably reduced by the presence of the boundary layer ahead of the porous material.

(3) Flows with Mach number variations of ± 0.01 along the center line of a fixed-geometry tunnel were obtained throughout the speed range of the tests ($M = 0.99$ to 1.17) by removal of air through commercial grade sintered bronze walls.

Langley Aeronautical Laboratory
National Advisory Committee for Aeronautics
Langley Air Force Base, Va.

REFERENCES

1. Evvard, John C., and Wyatt, DeMarquis D.: Investigation of a Variable Mach Number Supersonic Tunnel with Nonintersecting Characteristics. NACA RM E8J13, 1948.

2. Allen, H. Julian: The Asymmetric Adjustable Supersonic Nozzle for Wind-Tunnel Application. NACA RM A8E17, 1948.

3. Frick, Charles W., and Olson, Robert N.: Flow Studies in the Asymmetric Adjustable Nozzle of the Ames 6- by 6-Foot Supersonic Wind Tunnel. NACA RM A9E24, 1949.

4. Cooper, Morton, Smith, Norman F., and Kainer, Julian H.: A Pressure-Distribution Investigation of a Supersonic Aircraft Fuselage and Calibration of the Mach Number 1.59 Nozzle in the Langley 4- by 4-Foot Supersonic Tunnel. NACA RM L9E27a, 1949.

5. Puckett, Allen E.: Performance of the 12-Inch Wind Tunnel. Memo. 4-52, Jet Propulsion Lab., CIT, 1949.

6. Wright, Ray H., and Ward, Vernon G.: NACA Transonic Wind-Tunnel Test Sections. NACA RM L8J06, 1948.

7. Nelson, William J., and Bloetscher, Frederick: Preliminary Investigation of a Variable Mach Number Two-Dimensional Supersonic Tunnel of Fixed Geometry. NACA RM L9D29a, 1949.

8. Bates, George P.: Preliminary Investigation of 3-Inch Slotted Transonic Wind-Tunnel Test Sections. NACA RM L9D18, 1949.

9. Scroggs, A. M.: Data Report - Boeing Wind Tunnel Test No. 115 - Test No. 1 of the Slotted Test Sections in the $\frac{1}{20}$ Scale Model Wind Tunnel. Document No. D-9400, Boeing Airplane Co., Jan. 27, 1949.

10. Ferri, Antonio: Elements of Aerodynamics of Supersonic Flow. The Macmillan Co., 1949.

11. Burcher, Marie A.: Compressible Flow Tables for Air. NACA TN 1592, 1948.

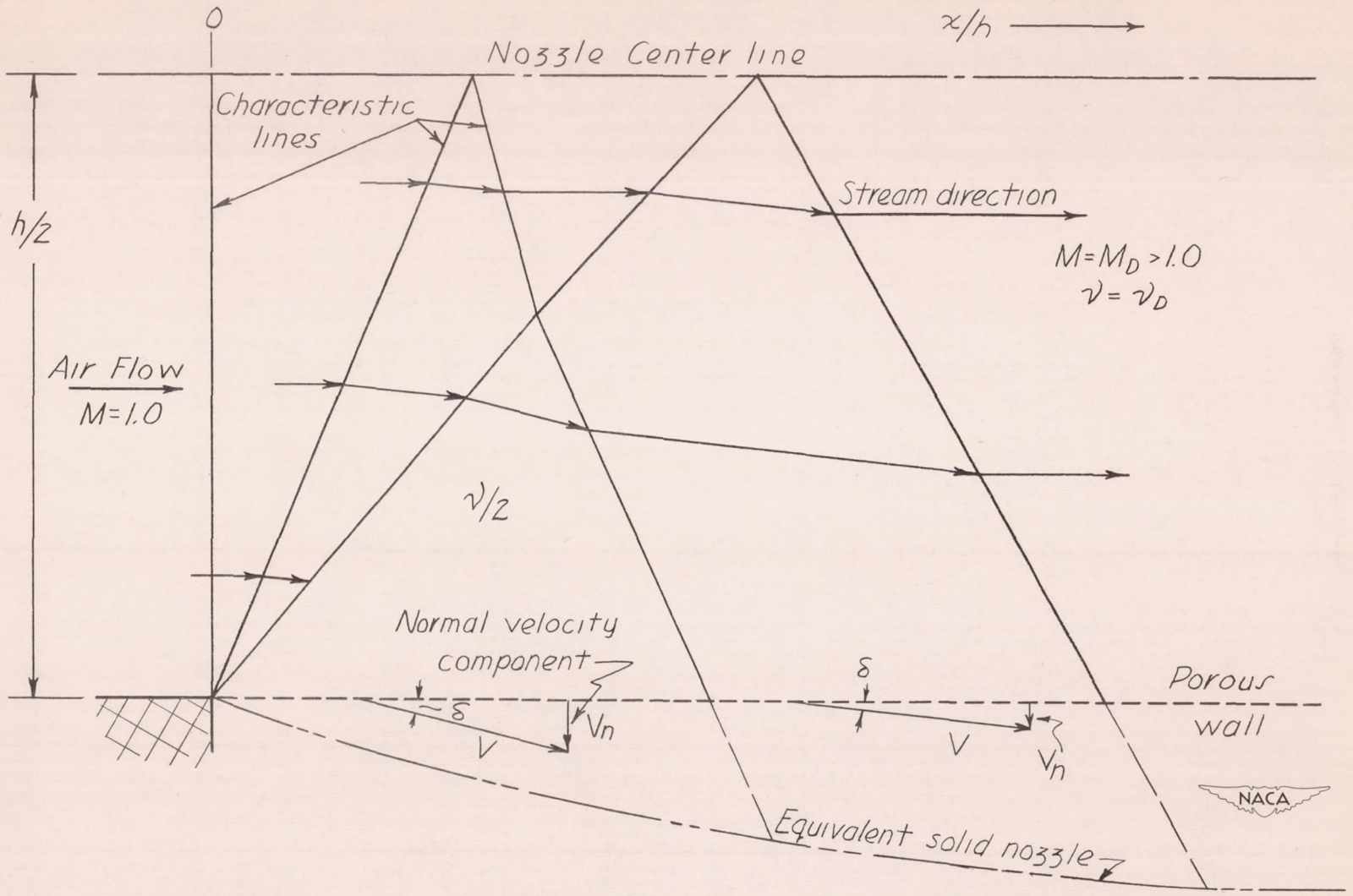

Figure 1.- Characteristic diagram.

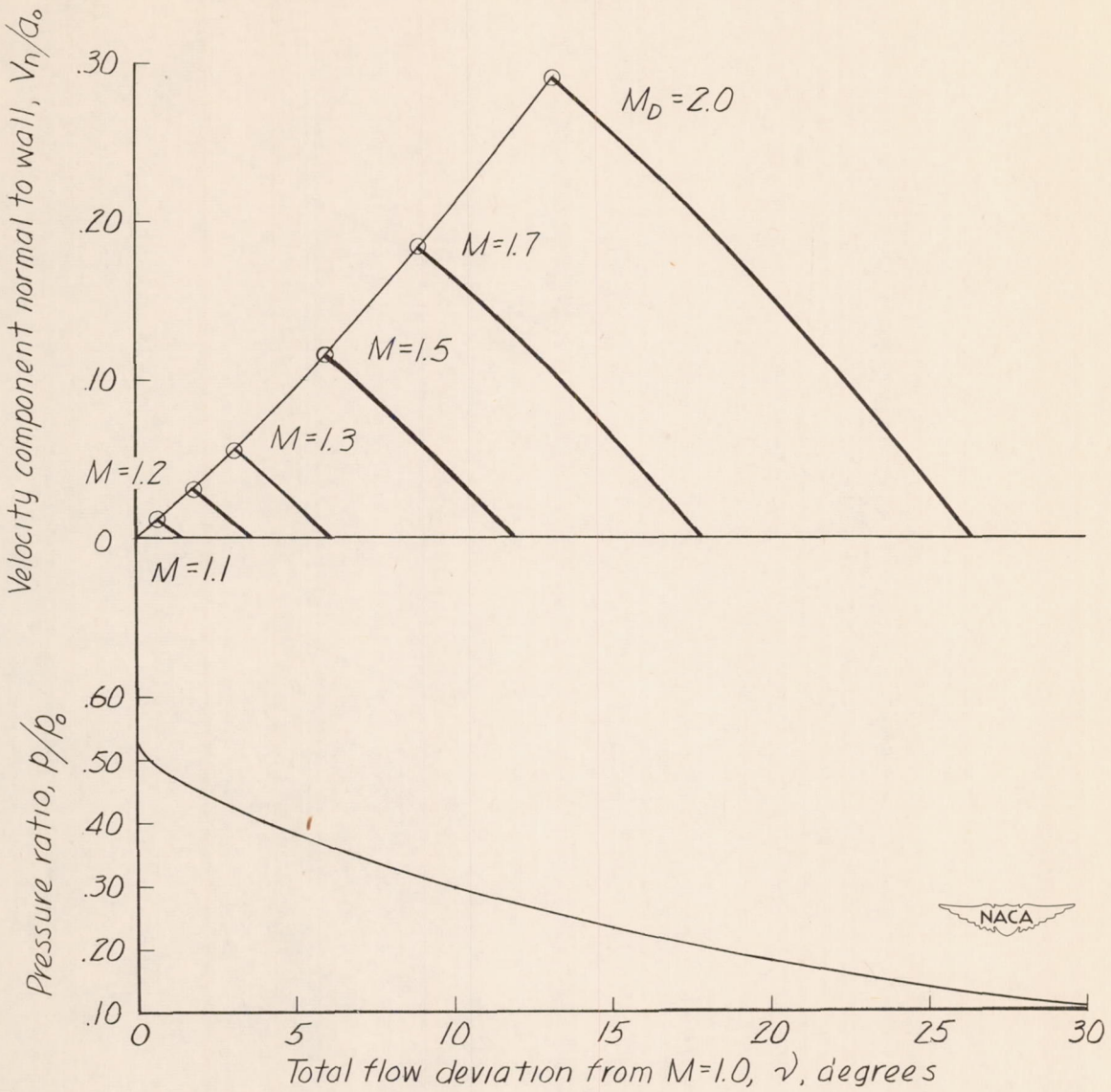

(a) V_n/a_o and p/p_o against ν.

Figure 2.- Flow conditions for shock-free nozzles.

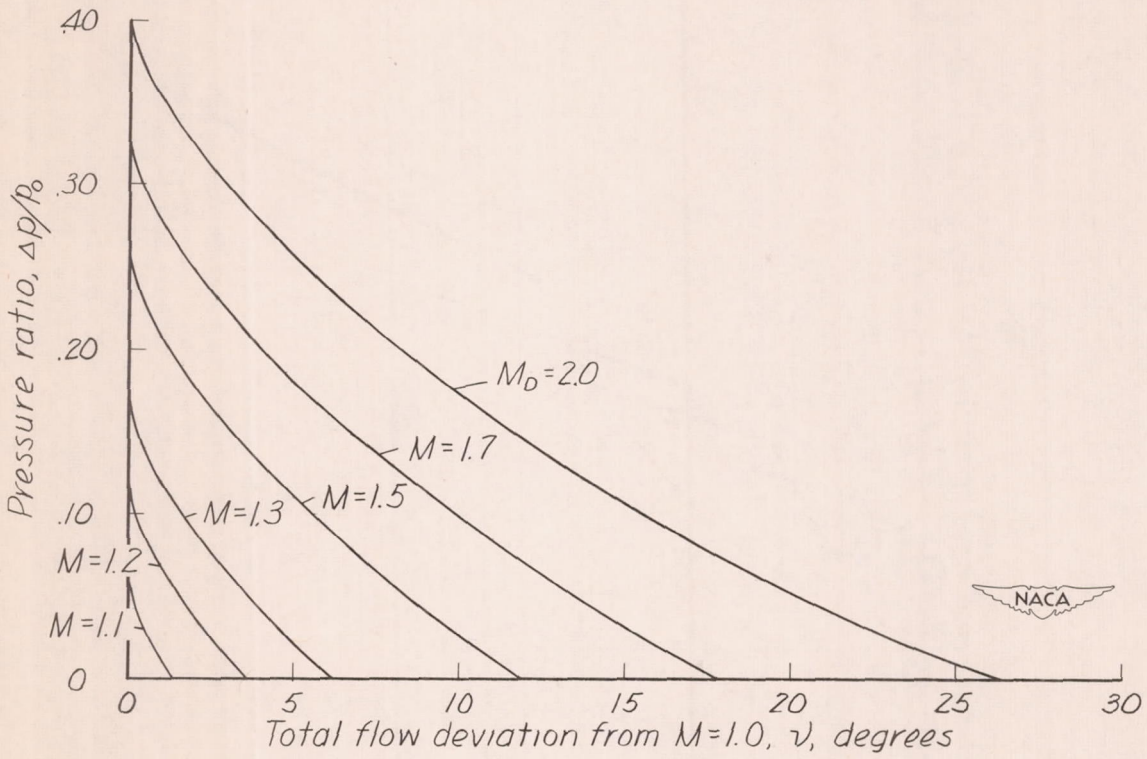

(b) $\Delta p/p_o$ against ν.

Figure 2.- Concluded.

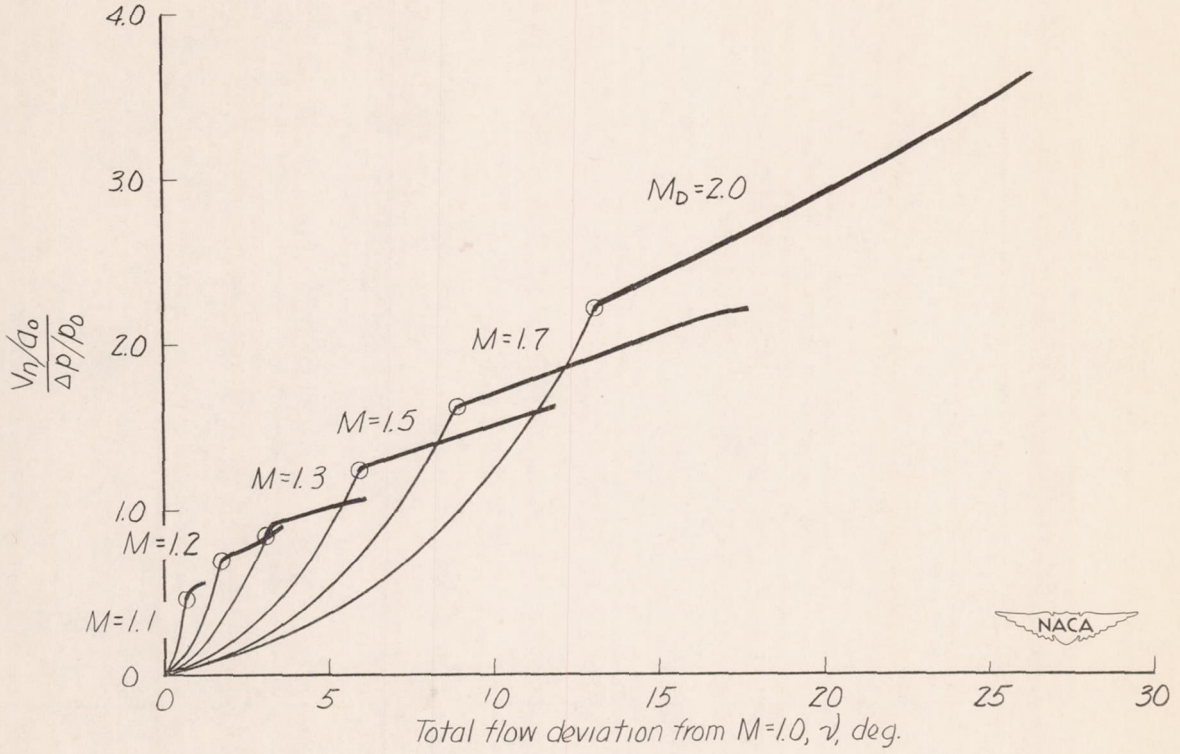

(a) $\frac{V_n/a_o}{\Delta p/p_o}$ against ν.

Figure 3.- Porosity requirement for shock-free flow.

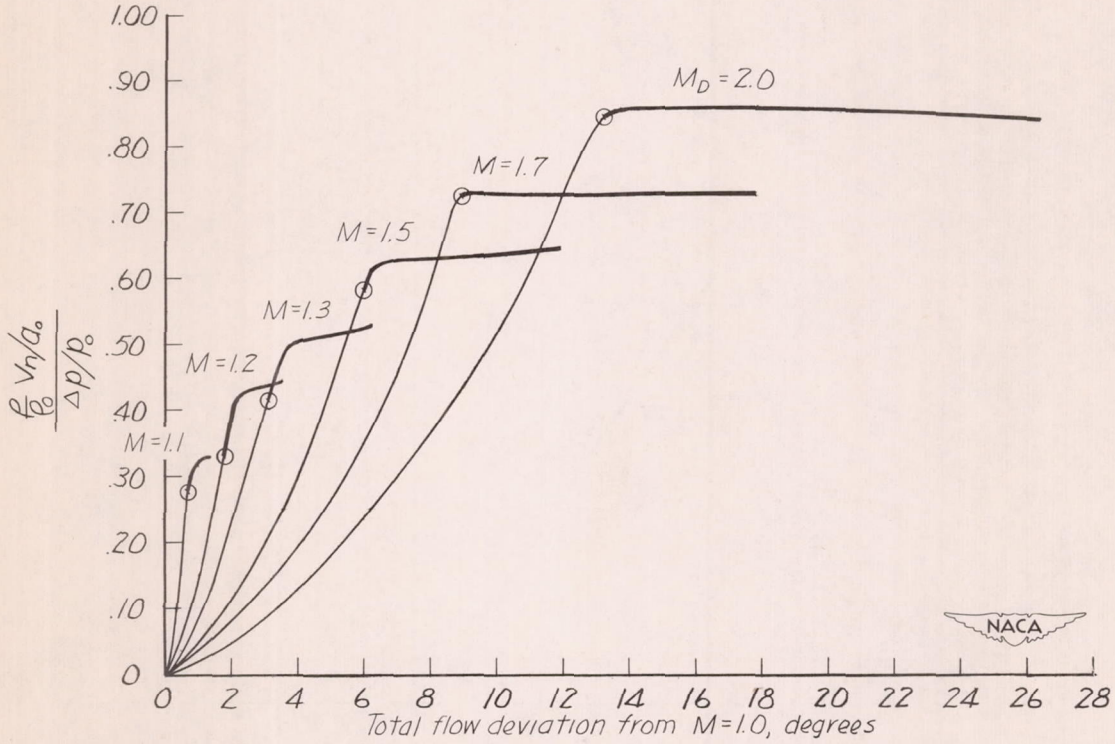

(b) $\dfrac{\frac{\rho}{\rho_o} v_n/a_o}{\Delta p/p_o}$ against ν.

Figure 3.- Continued.

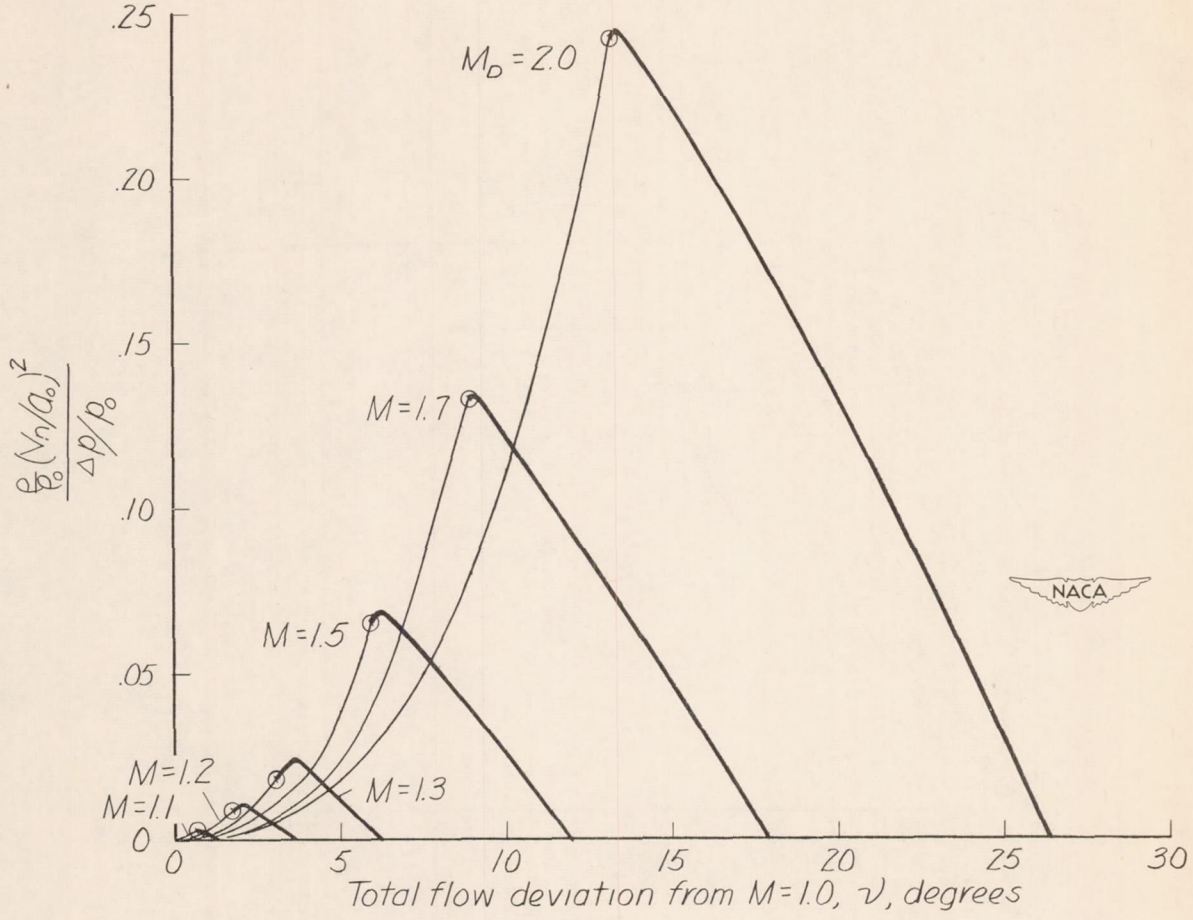

(c) $\frac{\frac{\rho}{\rho_o}\left(V_n/a_o\right)^2}{\Delta p/p_o}$ against ν.

Figure 3.- Concluded.

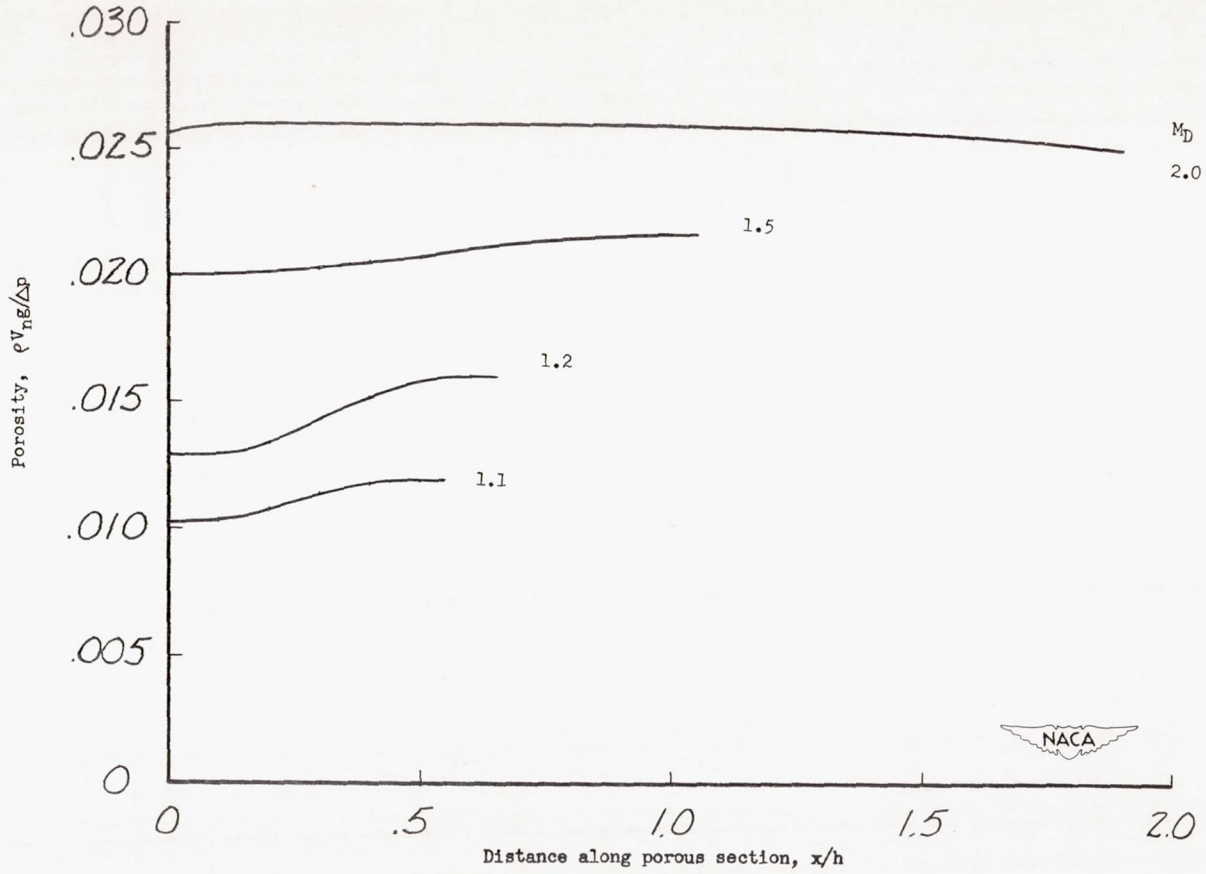

Figure 4.- Required porosity distribution for minimum-length shock-free nozzles. T_o = 500° R.

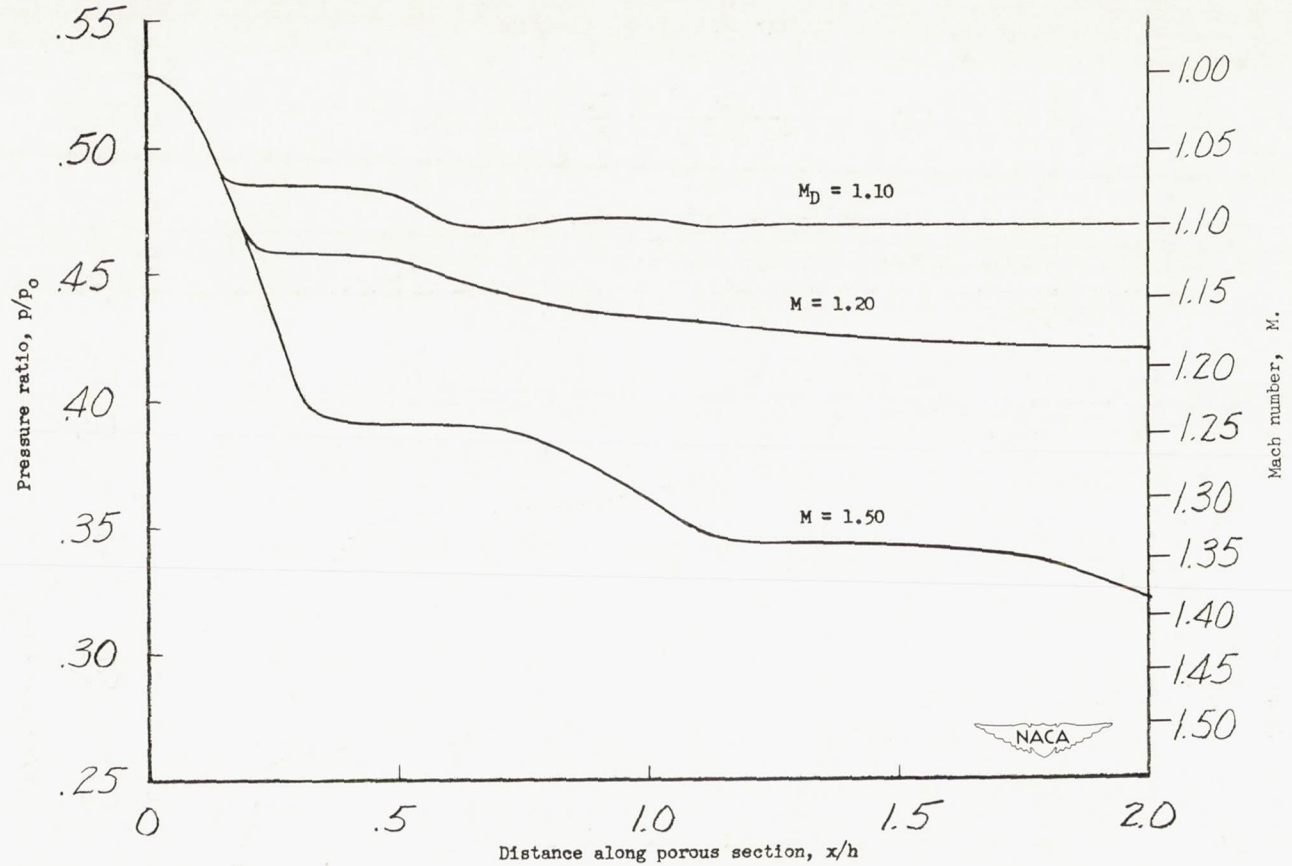

(a) $\left(\frac{\rho V_n g}{\Delta p}\right)_{500} \sqrt{\frac{500}{T_o}} = 0.0055.$

Figure 5.- Theoretical center-line pressure distributions for several Mach numbers and a constant $\rho V_n g/\Delta p$. $T_o = 500^\circ$ R.

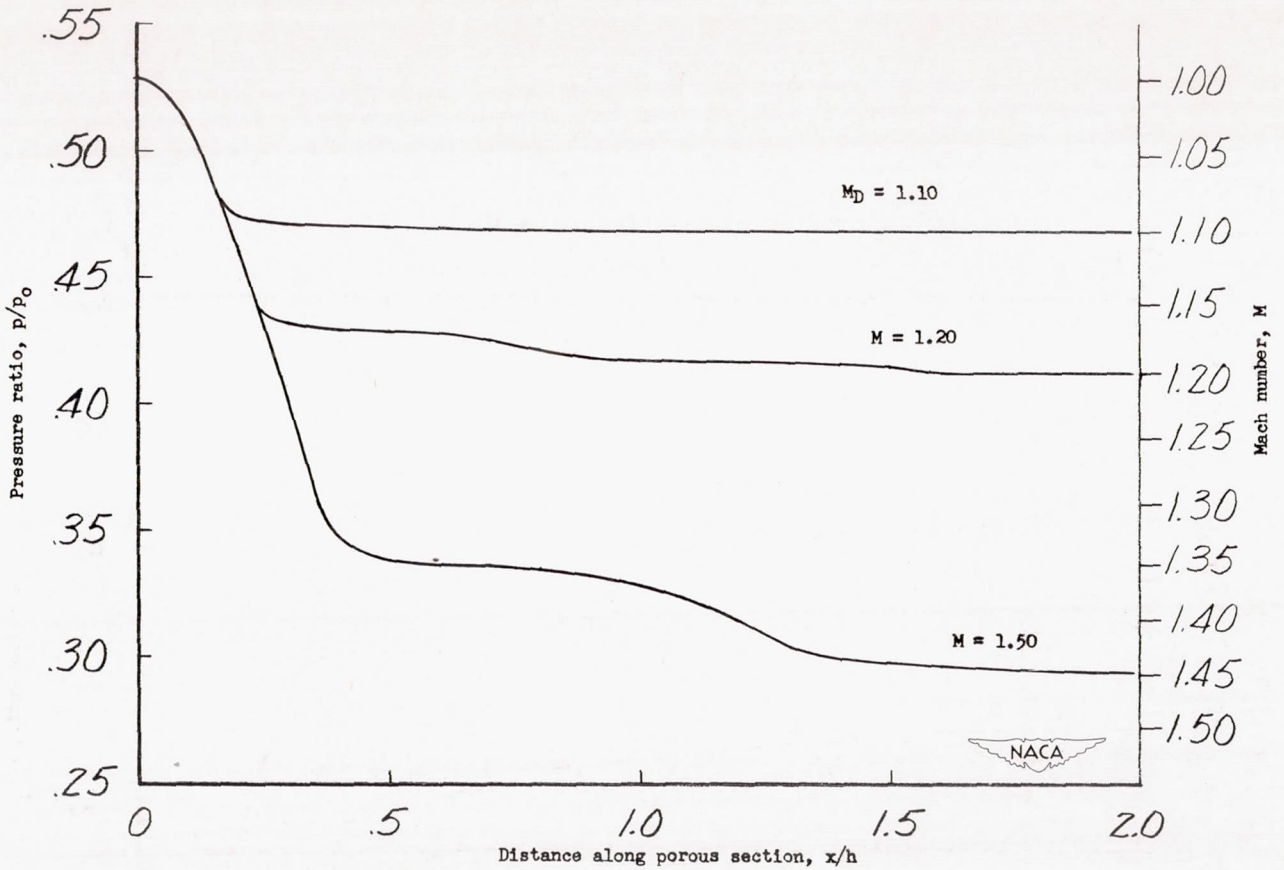

(b) $\left(\frac{\rho V_n g}{\Delta p}\right)_{500} \sqrt{\frac{500}{T_o}} = 0.011.$

Figure 5.- Continued.

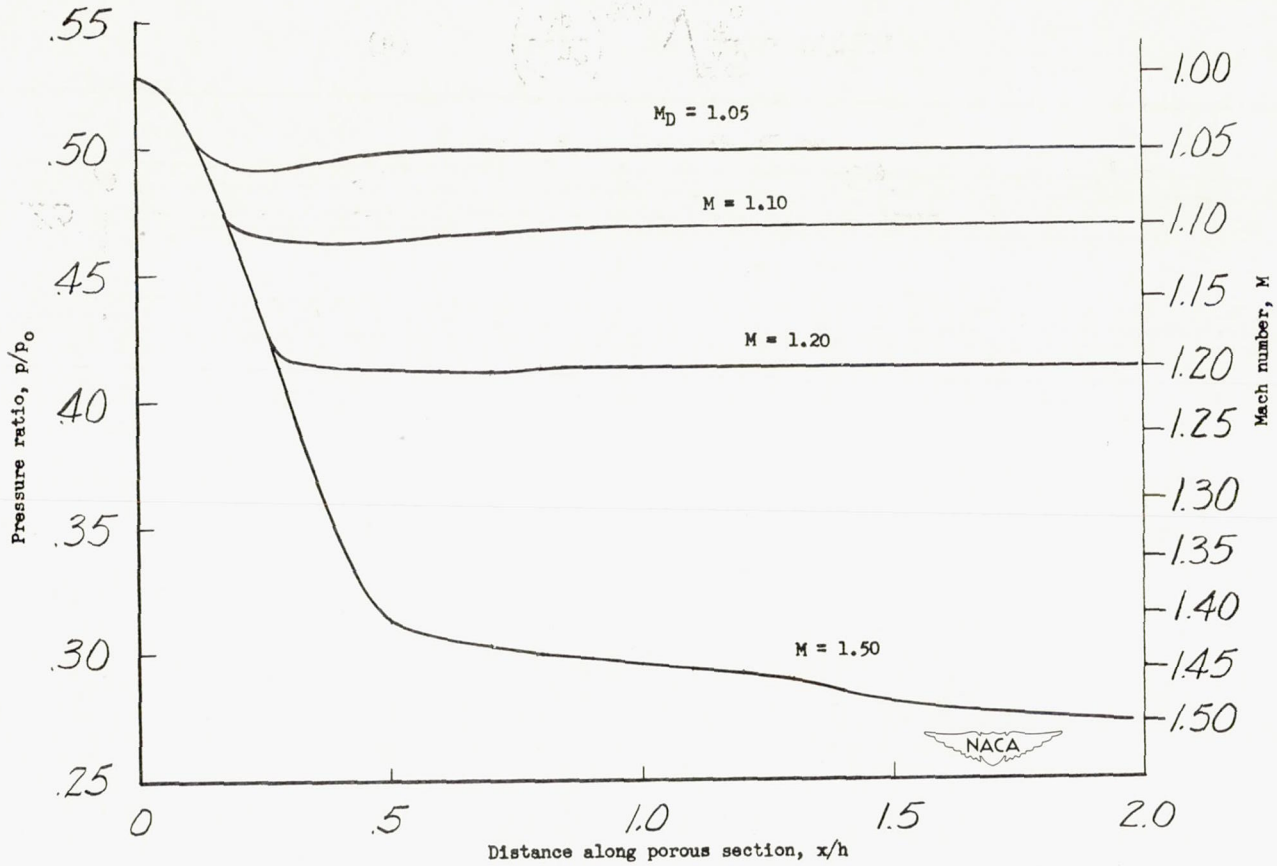

(c) $\left(\frac{\rho V_n g}{\Delta p}\right)_{500}\sqrt{\frac{500}{T_o}} = 0.018.$

Figure 5.- Concluded.

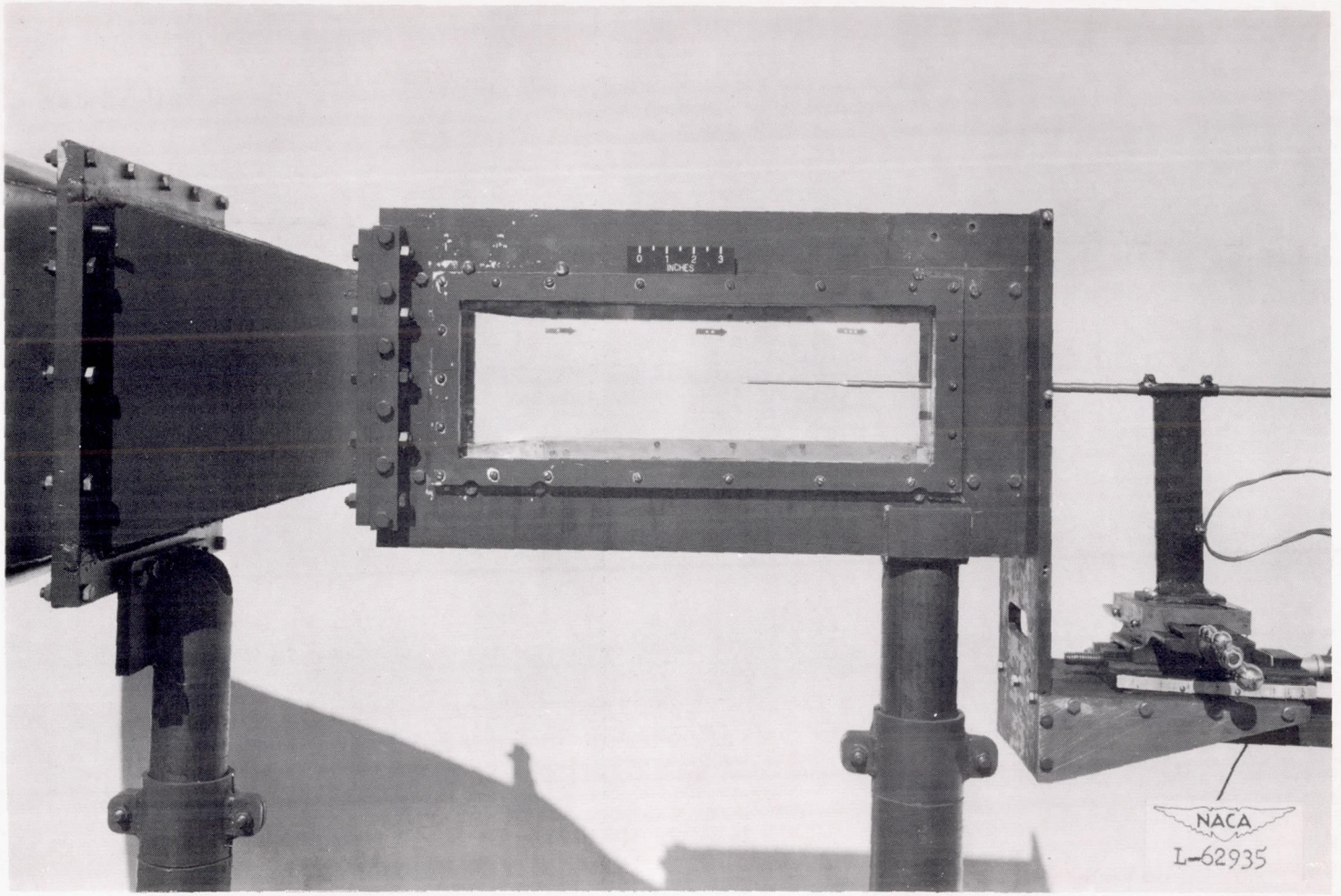

Figure 6.- General arrangement of experimental setup.

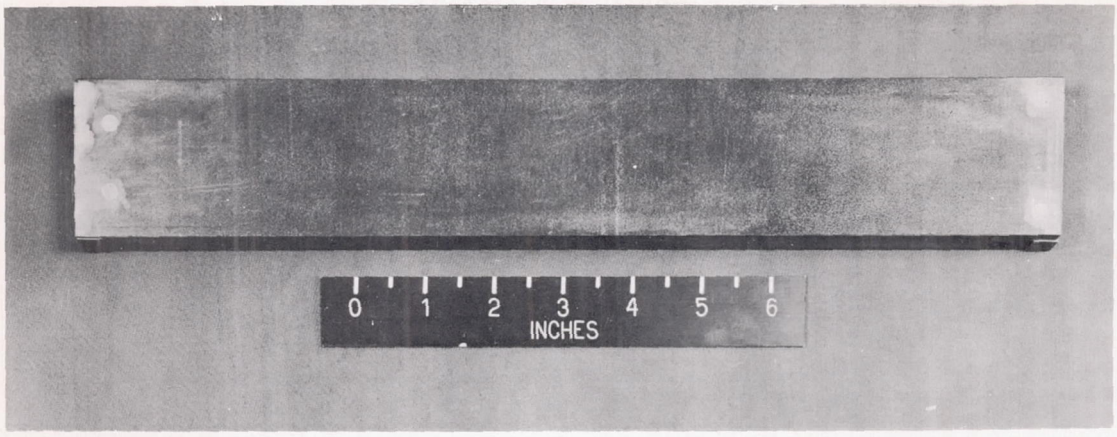

(a) Top view of sintered-bronze floor.

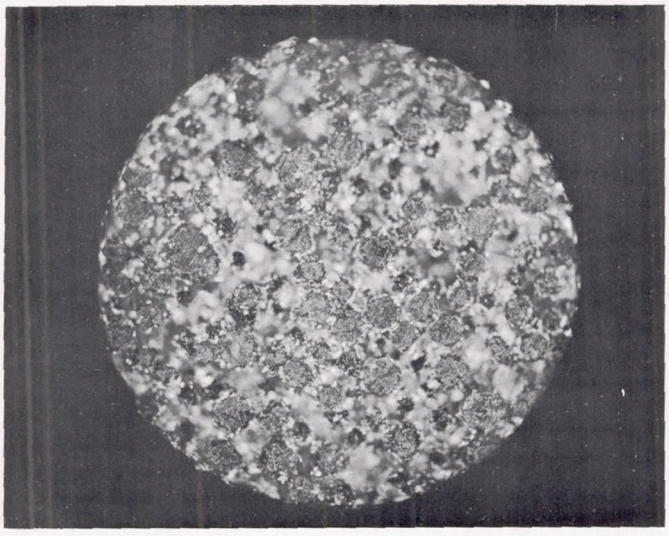

(b) Photomicrogram of sintered floor enlarged 25 diameters.

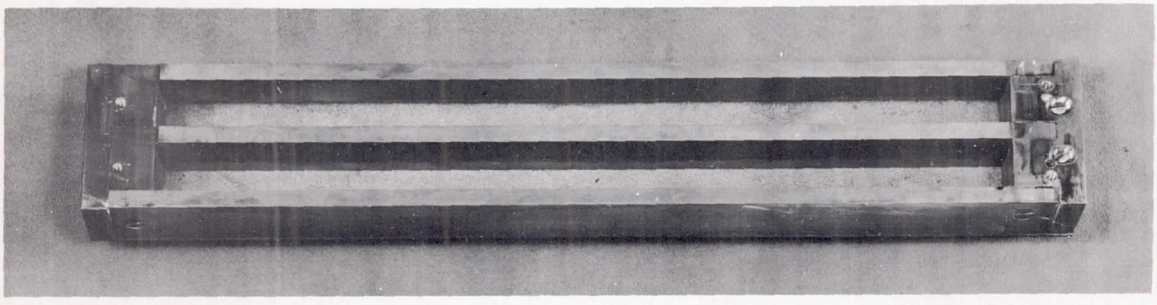

(c) Bottom view of sintered-bronze floor showing lateral supports.

Figure 7.- Porous sintered-bronze floor.

NACA
L-62201

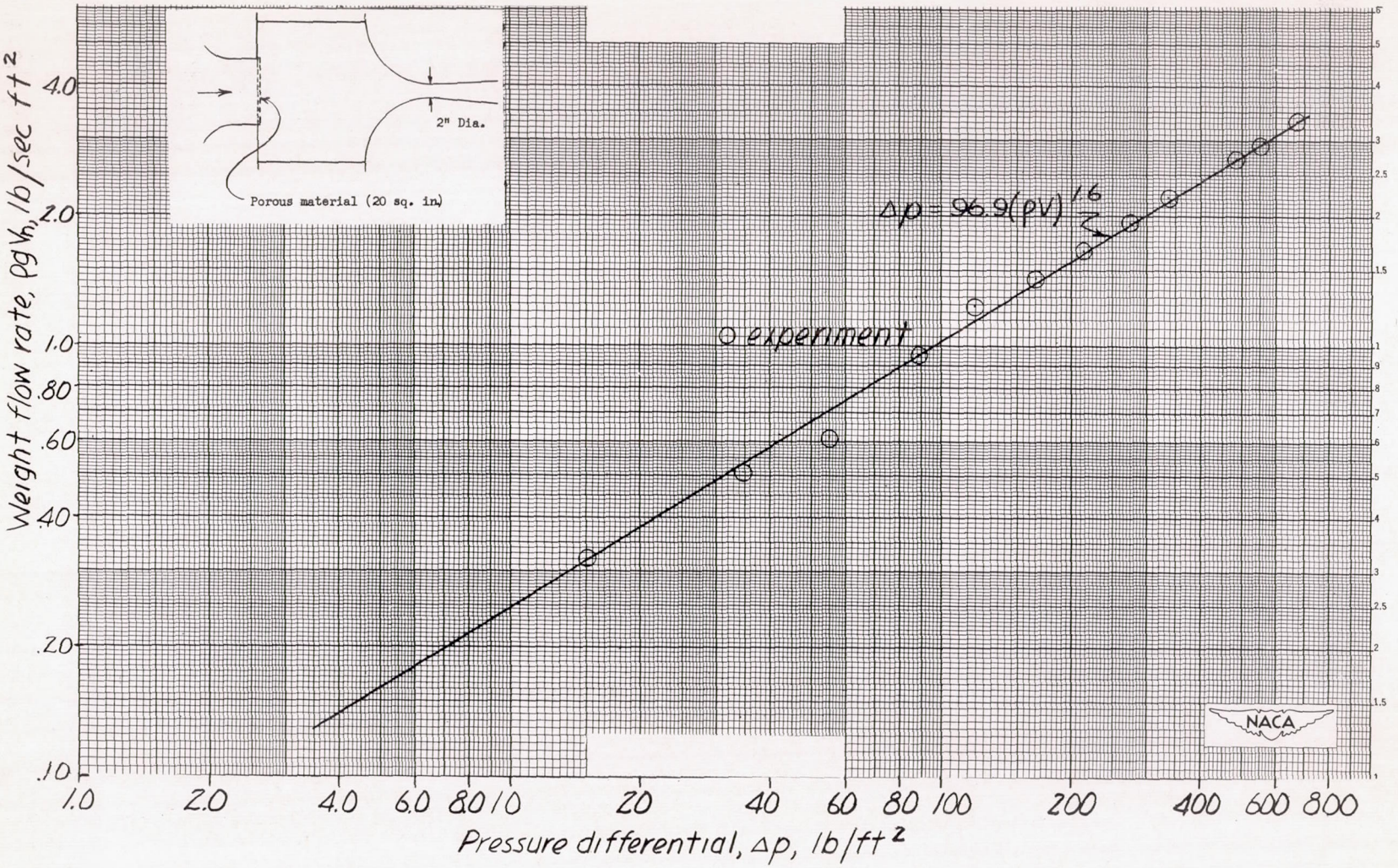

Figure 8.- Porosity calibration of sintered bronze used in walls of experimental channel.

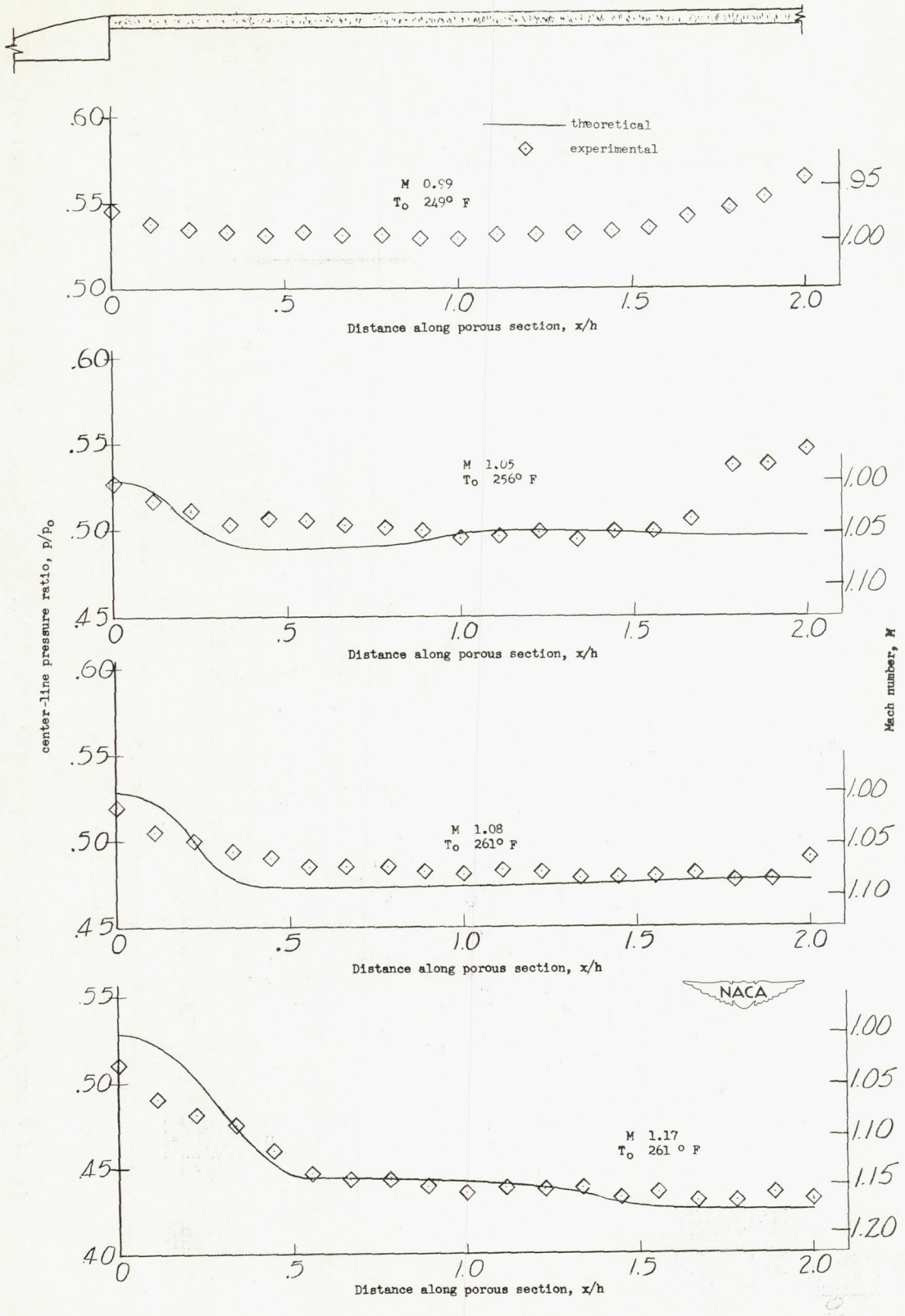

Figure 9.- Pressure distribution along center line of $2\frac{1}{4}$- by $4\frac{1}{2}$-inch porous-wall tunnel.

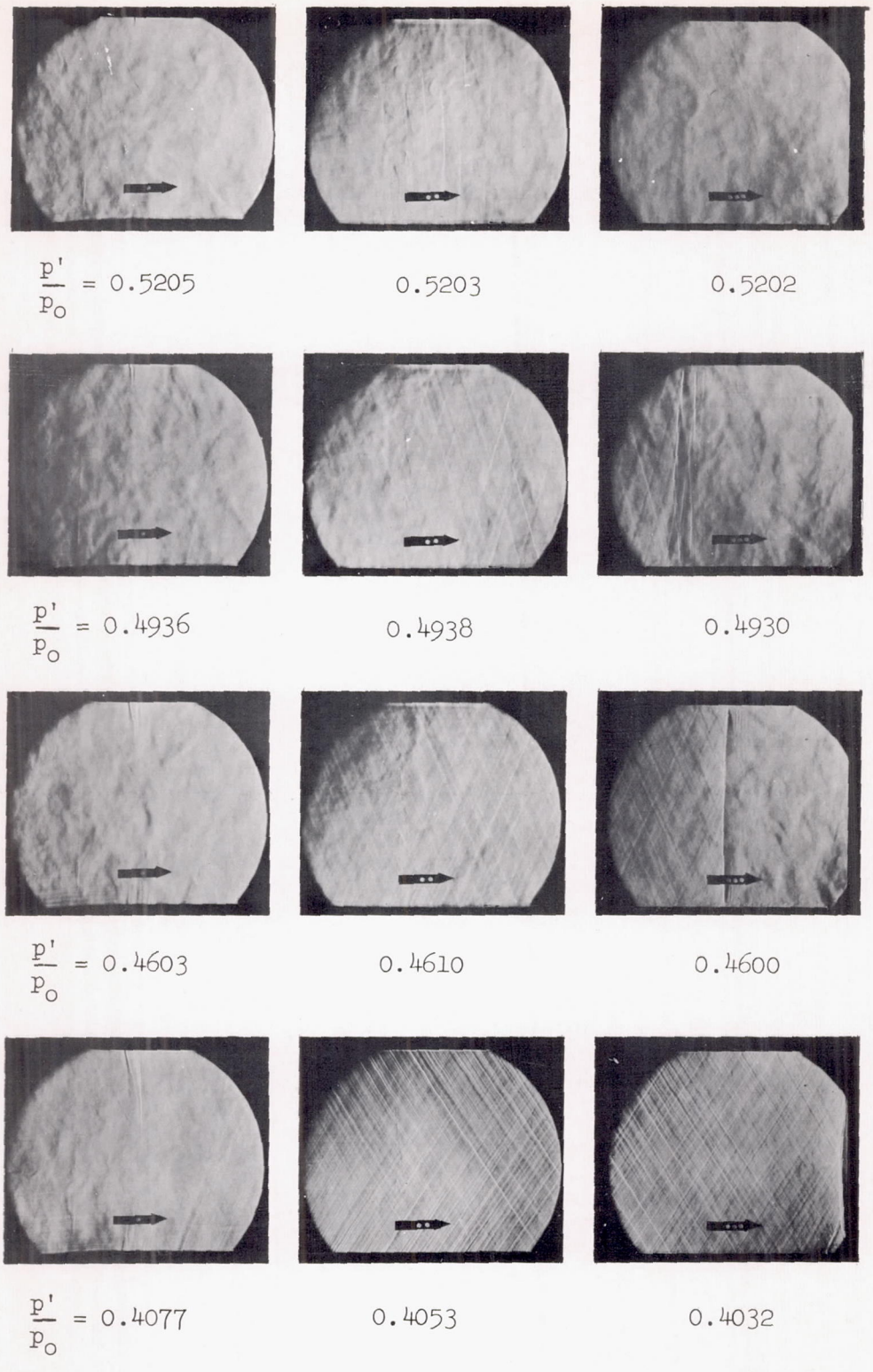

Figure 10.- Schlieren photographs of flow along $2\frac{1}{4}$- by $4\frac{1}{2}$-inch porous-wall tunnel.